Sound radiation from a cylindrical shell with a multilayered resonant coating

Cikai Lin, Gyani Shankar Sharma, Daniel Eggler, Laurent Maxit, Alex Skvortsov, Ian Macgillivray, Nicole Kessissoglou

Sound radiation from a cylindrical shell with a multilayered resonant coating

Cikai Lin,[1] Gyani Shankar Sharma,[1] Daniel Eggler,[1] Laurent Maxit,[2]
Alex Skvortsov,[3] Ian MacGillivray,[3] Nicole Kessissoglou[1]

[1]*School of Mechanical and Manufacturing Engineering, The University of New South Wales, Sydney, Australia*

[2]*Univ Lyon, INSA Lyon, LVA, 25 bis, av. Jean Capelle, F-69621, Villeurbanne Cedex, France*

[3]*Maritime Division, Defence Science and Technology, Melbourne, Australia*

Abstract

The vibroacoustic response of a structurally excited cylindrical shell submerged in water is presented. The shell is coated with a soft elastic material embedded with circumferential arrays of resonant inclusions. The coating is modelled as a multilayered equivalent fluid composed of homogeneous layers of the host soft material and homogenised layers comprising voids or hard inclusions. The radiated acoustic pressure is analytically derived by assembling and solving continuity and kinematic conditions at the interfaces between the cylindrical shell and the multilayered coating. Coating designs with different combinations of homogenised layers are examined. Physical mechanisms governing acoustic performance of the various coating designs are described. We show that the material of the inclusions, tuning the local resonances of the inclusions and the distribution of the homogenised layers within the coating have a significant effect on the shell vibroacoustic response.

1. Introduction

Cylindrical shells are found in a wide range of engineering applications such as an aircraft fuselage, pressure hull of an underwater vehicle, pressure vessels and pipelines. Prediction of the structural and acoustic responses of cylindrical shells is important for targeted noise and vibration mitigation strategies to reduce structural fatigue and structure-borne sound. Numerous approaches have been investigated to attenuate the vibroacoustic response of a cylindrical shell in air. Porous materials interlayered within the double walls of a cylindrical shell are commonly employed to enhance sound transmission loss through a shell structure subject to external flow conditions [1-10]. A reduction in sound transmission has also been achieved using local resonators to target the ring frequency and mass-spring-mass resonance of a double-walled cylindrical shell [11-14]. Coatings composed of orthotropic layers [15-18] or constrained damping layers [19-21] have been

utilised to effectively suppress the vibroacoustic response of a cylindrical shell. Piezoelectric material has also been applied as patches [22-24] or as a full coating [25,26] to actively attenuate the sound radiation from a cylindrical shell.

For underwater applications, a homogeneous viscoelastic coating applied to the wetted surface of a submerged shell has been shown to reduce acoustic scattering and radiation due to external acoustic sources [27-33]. Such coatings are generally made from a soft compliant material with an impedance match with water, which enhances its ability to absorb water-borne sound waves. A homogeneous viscoelastic coating has also been shown to attenuate the vibroacoustic response of a structurally excited submerged shell [33-35]. In addition to homogeneous materials, sound absorbing materials with resonant inclusions have been employed as acoustic coatings for reduction of underwater noise [36-69]. The main mechanism for sound attenuation arises from increased wave scattering and the associated strain field amplification near inclusions at frequencies around local resonance of the inclusions. This behaviour facilitates conversion of sound waves into shear waves which are efficiently absorbed due to high shear damping of the coating. Tailored noise control can be achieved by tuning the local resonance frequency of the inclusions, which in turn is achieved by varying the size, shape and proximity of the inclusions [36-40]. There is a plethora of literature on the acoustic performance of coatings with resonant inclusions spanning analytical approaches based on homogenisation theory [36-42], multiple scattering theory [43-46] and resonance scattering theory [47,48]. Numerical models developed using the finite element method [49-63], as well as numerous experimental studies on coatings for maritime applications have also been reported [64-69].

Early works on acoustic coatings considered periodic voids for which the local resonance of the inclusions is monopolar [36-38,43,48]. Acoustic coatings comprising hard inclusions, for which the local resonance of the scatterers is dipolar, have shown consistent sound absorption performance under hydrostatic pressure [39,44,49,64]. While the majority of studies considered coatings embedded with inclusions of the same material, few papers have studied inclusions of different materials, namely voids and resonant scatterers [70,71]. Further, the aforementioned studies on resonant coatings submerged in water examined planar structures. We recently showed that a coating composed of a layer of voids can reduce radiated sound from a coated cylindrical shell over a broad frequency range around monopole resonance of the voids [72]. In another recent study, Ke et al. [73] employed the finite element method to identify the effective parameters of a coating on the external surface of an elastic spherical shell. A reduction in target strength for the coated shell compared to an uncoated shell was observed.

The current paper investigates the acoustic performance of a multilayered coated cylindrical shell with resonant inclusions of different materials. The coating is modelled as an equivalent fluid composed of alternating homogeneous and homogenised layers. The effective material and

geometric properties for the homogenised circumferential layer of resonant inclusions are approximated using the effective properties for a planar array of resonant inclusions in a square lattice. This approach is shown to be valid when the radius of the cylindrical shell is much greater than the diameter of the inclusions and spacing between adjacent inclusions. The vibroacoustic response of the coated cylindrical shell is obtained by assembling and solving continuity and kinematic boundary conditions at the interface between contacting layers. We first compare the acoustic performance of a coating with a single homogenised layer of voids or hard inclusions. We then investigate the acoustic performance of a coating with several homogenised layers composed of voids and/or hard inclusions. The material of the inclusions as well as the distribution of the homogenised layers within the coating have a large impact on the vibroacoustic response of a submerged coated shell. We show that the radiated sound can be significantly attenuated by tuning the local resonances of the inclusions to targeted frequencies by varying the geometric values of the resonant inclusions.

2. Analytical formulation

This section describes the analytical formulation to predict the vibroacoustic response of a coated cylindrical shell. Figure 1(a) schematically shows a cylindrical shell of infinite length with mean radius a and thickness h_s. The shell is submerged in a heavy fluid of density ρ_{ext} and speed of sound c_{ext}. The interior domain has density ρ_{int} and speed of sound c_{int}. The shell is coated with a soft elastic medium of density ρ_c, longitudinal modulus κ_c and thickness h_c. Cylindrical-shaped resonant inclusions are embedded in the centre of the coating and equispaced along the circumference by distance d. The layer of resonant inclusions can be represented as a homogenised layer with effective material and geometric properties, as shown in Fig. 1(b). The analytical methodology presents the equations of motion for the cylindrical shell, general solutions for the shell displacements, acoustic pressures in the multilayered coating and in the interior and exterior fluid domains, and continuity equations at interfaces between the fluid domains, shell surfaces and coating layers.

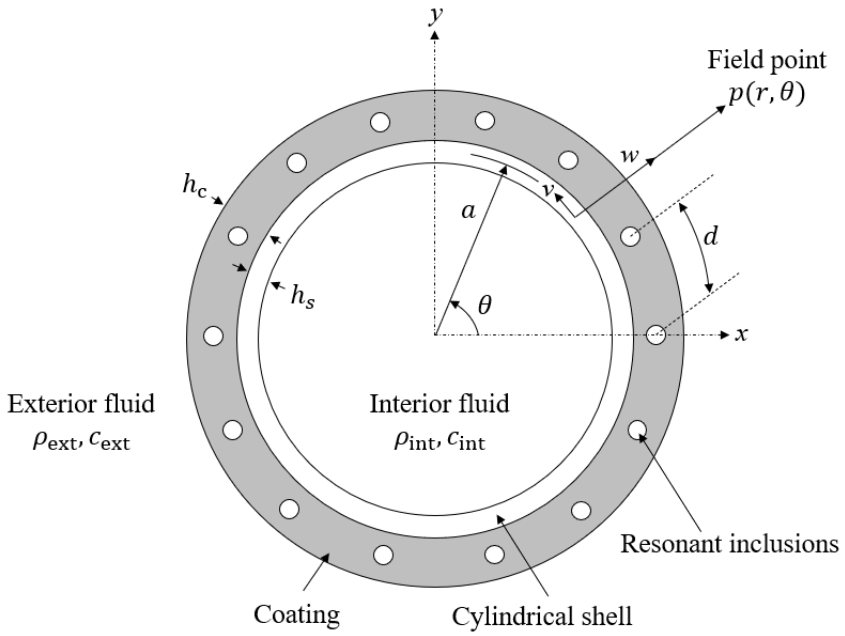

(a)

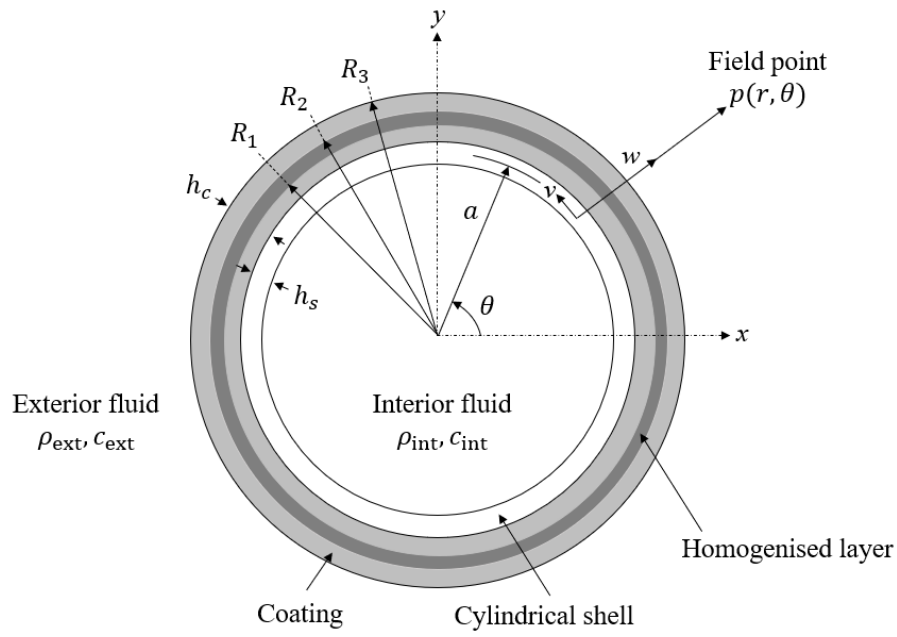

(b)

Figure 1 Schematic diagram of a cylindrical shell with a soft elastic coating embedded with (a) equispaced resonant inclusions and (b) a homogenised layer (not to scale).

2.1 Shell equations of motion

The equations of motion for the cylindrical shell are based on Donnell-Mushtari theory with a modifying operator by Flügge-Byrne-Lur'ye. The geometric and material properties of the shell as well as the structural forcing are considered invariant along the axial direction and as such, the problem studied here is reduced to two dimensions. The shell is excited by a radial line force applied to the interior surface of the shell. Using the time-harmonic convention $e^{-\mathrm{i}\omega t}$ where $\mathrm{i} = \sqrt{-1}$ and ω is the angular frequency, the equations of motion of the shell are given by [74]

$$\frac{D}{a^4}\left(\frac{d^4}{d\theta^4} + 2\frac{d^2}{d\theta^2} + 1 + \beta^2 - \frac{\omega^2\rho_s h_s a^4}{D}\right)w(\theta) + \frac{D\beta^2}{a^4}\frac{dv}{d\theta}(\theta) = p_{\mathrm{int}}(a,\theta) - p_1(a,\theta) + F(\theta) \tag{1}$$

$$\frac{G}{a^2}\frac{dw}{d\theta}(\theta) + \frac{G}{a^2}\left(\frac{d^2}{d\theta^2} + \frac{\omega^2\rho_s h_s a^2}{G}\right)v(\theta) = 0, \tag{2}$$

where w and v are the shell radial and tangential displacements, respectively. $D = \frac{E_s h_s^3}{12(1-\upsilon_s^2)}$ is the flexural stiffness of the shell, $G = \frac{E_s h_s}{(1-\upsilon_s^2)}$ is the shell extensional stiffness, $\beta = \frac{\sqrt{12}a}{h_s}$ is the dimensionless shell thickness parameter, E_s is the complex Young's modulus that incorporates the structural loss factor, ρ_s is the density and υ_s is Poisson's ratio of the shell. The right hand side of Eq. (1) represents the various loads acting on the shell surface, corresponding to the acoustic pressure of the interior field denoted by $p_{\mathrm{int}}(a,\theta)$, the acoustic pressure at the interface of the shell and the coating denoted by $p_1(a,\theta)$, and the radial line force $F(\theta)$.

2.2 General solutions

Using a Fourier series expansion, general solutions for the radial and tangential shell displacements are given by

$$w(\theta) = \sum_{n=-\infty}^{\infty} w_n\, e^{\mathrm{i}n\theta}, \tag{3}$$

$$v(\theta) = \sum_{n=-\infty}^{\infty} v_n\, e^{\mathrm{i}n\theta}, \tag{4}$$

where w_n and v_n are Fourier coefficients associated with the shell displacements. The interior and exterior acoustic pressure fields can also be expressed in terms of a Fourier series expansion as [75]

$$p_{\text{int}}(r,\theta) = \sum_{n=-\infty}^{\infty} P_{n,\text{int}} J_n(k_{\text{int}} r)\, e^{\text{i}n\theta}, \tag{5}$$

$$p_{\text{ext}}(r,\theta) = \sum_{n=-\infty}^{\infty} P_{n,\text{ext}} H_n^1(k_{\text{ext}} r)\, e^{\text{i}n\theta}, \tag{6}$$

where $P_{n,\text{int}}$ and $P_{n,\text{ext}}$ are unknown scattering coefficients for the interior and exterior acoustic fields. J_n and H_n^1 are the Bessel and Hankel functions of the first kind of order n. k_{int} and k_{ext} ($k = \omega/c$) denote the acoustic wave number in the interior and exterior acoustic fields, respectively.

Representing the coating as a three-layered equivalent fluid, general solutions for the acoustic pressures in the inner layer, homogenised layer and outer layer of the coating are respectively given by

$$p_1(r,\theta) = \sum_{n=-\infty}^{\infty} \left(a_{n,1} J_n(k_c r) + b_{n,1} H_n^1(k_c r)\right) e^{\text{i}n\theta}, \tag{7}$$

$$p_2(r,\theta) = \sum_{n=-\infty}^{\infty} \left(a_{n,2} J_n(k_{\text{eff}} r) + b_{n,2} H_n^1(k_{\text{eff}} r)\right) e^{\text{i}n\theta}, \tag{8}$$

$$p_3(r,\theta) = \sum_{n=-\infty}^{\infty} \left(a_{n,3} J_n(k_c r) + b_{n,3} H_n^1(k_c r)\right) e^{\text{i}n\theta}, \tag{9}$$

where $(a_{n,1}, b_{n,1})$, $(a_{n,2}, b_{n,2})$, $(a_{n,3}, b_{n,3})$ are unknown scattering coefficients in the inner, homogenised and outer layers of the coating, respectively. $k_c = \omega/\sqrt{\kappa_c/\rho_c}$ and $k_{\text{eff}} = \omega/\sqrt{\kappa_{\text{eff}}/\rho_{\text{eff}}}$ respectively correspond to the acoustic wave number in the homogeneous and homogenised layers. The effective material properties $(\rho_{\text{eff}}, \kappa_{\text{eff}})$ in the homogenised layers composed of voids or hard inclusions are given in Appendix A.

2.3 Shell excitation

The shell is excited by a radial line force given by

$$F(\theta) = F_r \delta\big(a(\theta - \theta_r)\big), \tag{10}$$

where θ_r is the angular location of the force, F_r is the radial force amplitude and $\delta\big(a(\theta - \theta_r)\big)$ is the Dirac delta function. Using a Fourier series expansion and the identity given by $\delta(a\theta) = \delta(\theta)/|a|$, the Dirac delta function can be expressed as

$$\delta\big(a(\theta - \theta_r)\big) = \sum_{n=-\infty}^{\infty} \left(\frac{1}{2\pi a} \int_0^{2\pi} \delta(\theta - \theta_r) e^{-\text{i}n\theta} d\theta\right) e^{\text{i}n\theta}. \tag{11}$$

Substituting Eq. (11) into Eq. (10) and simplifying yields the following expression for the radial line force

$$F(\theta) = \sum_{n=-\infty}^{\infty} \frac{F_r e^{-in\theta_r}}{2\pi a} e^{in\theta}. \tag{12}$$

2.4 Continuity conditions

The unknown coefficients are determined by satisfying continuity conditions at radial locations of a, R_1, R_2 and R_3. At $r = a$, the shell is coupled to both the interior acoustic pressure and inner surface of the coating by the following kinematic conditions

$$\frac{\partial p_{\text{int}}}{\partial r} = \omega^2 \rho_{\text{int}} w, \qquad r = a, \tag{13}$$

$$\frac{\partial p_1}{\partial r} = \omega^2 \rho_c w, \qquad r = a. \tag{14}$$

It should be herein noted that both Eqs. (13) and (14) incorporate Eq. (12) arising from a radial force applied to the interior surface of the shell. Continuity of acoustic pressure at radial locations of R_1, R_2, R_3 are given by

$$p_1 = p_2, \qquad r = R_1, \tag{15}$$

$$p_2 = p_3, \qquad r = R_2, \tag{16}$$

$$p_3 = p_{\text{ext}}, \qquad r = R_3. \tag{17}$$

Continuity of normal velocity at radial locations of R_1, R_2, R_3 are given by

$$\frac{1}{\rho_c}\frac{\partial p_1}{\partial r} = \frac{1}{\rho_{\text{eff}}}\frac{\partial p_2}{\partial r}, \qquad r = R_1, \tag{18}$$

$$\frac{1}{\rho_{\text{eff}}}\frac{\partial p_2}{\partial r} = \frac{1}{\rho_c}\frac{\partial p_3}{\partial r}, \qquad r = R_2, \tag{19}$$

$$\frac{1}{\rho_c}\frac{\partial p_3}{\partial r} = \frac{1}{\rho_{\text{ext}}}\frac{\partial p_{\text{ext}}}{\partial r}, \qquad r = R_3. \tag{20}$$

Equations (13)-(20) are assembled into a linear system of equations in matrix form expressed as $\mathbf{AX} = \mathbf{F}$, where $\mathbf{A}$ is an 8×8 matrix for which the non-zero terms are listed in Appendix B. $\mathbf{X}$ and $\mathbf{F}$ are coefficient and force vectors given by $\mathbf{X} = [a_{n,1} \quad b_{n,1} \quad a_{n,2} \quad b_{n,2} \quad a_{n,3} \quad b_{n,3} \quad P_{n,\text{int}} \quad P_{n,\text{ext}}]^{\text{T}}$ and $\mathbf{F} = \left[\frac{F_r e^{-in\theta_r}}{2\pi a} \quad \frac{F_r e^{-in\theta_r}}{2\pi a} \quad 0 \quad 0 \quad 0 \quad 0 \quad 0 \quad 0\right]^{\text{T}}$ where $^{\text{T}}$ represents the vector transpose. Solutions to the unknown coefficients are obtained from $\mathbf{X} = \mathbf{A}^{-1}\mathbf{F}$.

2.5 Homogeneous coated shell

For a cylindrical shell with a homogeneous coating (in the absence of resonant inclusions), Eqs. (7) to (9) are replaced by

$$p_c(r,\theta) = \sum_{n=-\infty}^{\infty} \left(a_n J_n(k_c r) + b_n H_n^1(k_c r)\right) e^{in\theta}. \tag{21}$$

Similarly, Eqs. (14)-(20) are replaced by continuity equations on the inner surface ($r = a$) and outer surface ($r = R$) of the coating as follows

$$\frac{\partial p_c}{\partial r} = \omega^2 \rho_c w, \qquad r = a, \tag{22}$$

$$p_c = p_{\text{ext}}, \qquad r = R, \tag{23}$$

$$\frac{1}{\rho_c}\frac{\partial p_c}{\partial r} = \frac{1}{\rho_{\text{ext}}}\frac{\partial p_{\text{ext}}}{\partial r}, \qquad r = R. \tag{24}$$

Following a similar procedure described previously, solutions to the unknown coefficients corresponding to a_n, b_n, $P_{n,\text{int}}$, $P_{n,\text{ext}}$ are obtained from assembling a linear system of equations ($\mathbf{AX} = \mathbf{F}$) and calculating the coefficients using $\mathbf{X} = \mathbf{A}^{-1}\mathbf{F}$.

3. Results and discussion

To understand the physical mechanisms governing the vibroacoustic response of a coated shell for a given inclusion material, a single homogenised layer of voids or hard inclusions embedded in the coating is initially studied. Multilayered coating designs using different combinations of homogenised layers composed of voids and/or hard inclusions are then examined.

3.1 Shell parameters

We model an infinitely long cylindrical shell of mean radius a = 1 m and thickness h_s = 0.01 m. The shell material is steel with density $\rho_s = 7800$ kg/m^3, Young's modulus $E_s = 210(1-0.02\text{i})$ GPa and Poisson's ratio $\upsilon_s = 0.3$. The shell is submerged in water with density ρ_{ext} = 1000 kg/m^3 and speed of sound c_{ext} = 1500 m/s. The external surface of the shell is coated with an elastic rubber-like material of density $\rho_c = 1000$ kg/m^3, longitudinal modulus $\kappa_c = 1(1\text{-}0.01\text{i})$ GPa, and shear modulus (second Lamé constant) $\mu_c = 0.6(1\text{-}0.3\text{i})$ MPa, in which the loss factor for the shear modulus is much larger than the loss factor for longitudinal modulus. The hard inclusions are steel with the same material properties as the shell. The voids are vacuous. The shell is excited by a radial line force with an amplitude of $F_r = 1$ N/m applied to its interior surface at θ_r = 0. Results

for the radiated pressure are obtained at a location of $(r, \theta) = (5a, \pi)$ downstream of the shell with respect to the force.

For validation of our analytical approach, a finite element model was developed in COMSOL Multiphysics v5.5 using the aforementioned material and geometric parameters for the coated cylindrical shell. The elastic coating and hard inclusions were modelled using the Solid Mechanics module. The exterior water domain was modelled using the Pressure Acoustics module. A free boundary condition was applied at the interior surface of the shell. Free boundary conditions were also applied at the interfaces between the voids and the coating. Continuity boundary conditions were applied at the interfaces between the hard inclusions and the coating. An acoustic-structure boundary condition was applied at the exterior surface of the coating to account for the interaction between the coated cylindrical shell and surrounding water. A perfectly matched layer was applied at the outer boundary of the exterior acoustic domain to ensure anechoic termination of outgoing acoustic waves. The acoustic and structural domains were meshed using free triangular elements and the perfectly matched layer was meshed using mapped quadrilateral elements. A minimum of six elements per wavelength at the highest frequency of 2 kHz was considered.

3.2 Single layer of resonant inclusions

We consider a coating of thickness h_c = 0.1 m and embedded with a single layer of resonant inclusions. For the coating with voids, 50 equispaced voids of 5 cm diameter were modelled, which yields a monopole resonance frequency predicted using Eq. (A5) of 486 Hz. For the coating with steel inclusions, 110 equispaced scatterers of 5 cm diameter were modelled, which yields a dipole resonance frequency predicted using Eq. (A8) of 519 Hz. For the number and size of inclusions considered here, the effective thickness is 15.9 mm for the homogenised layer of voids and 51.7 mm for the homogenised layer of hard inclusions. Figure 2 presents the radiated acoustic pressure from an uncoated shell and from a shell with a coating composed of a single layer of voids or hard inclusions, obtained analytically using the methodology presented in this work and numerically using the finite element method. The monopole and dipole resonances predicted analytically are indicated by circles. Discrepancies between analytical and numerical results for the locally resonant coated shells are attributed to the fact that effective material and geometric properties were used in the analytical model to characterise the homogenised layer (as per Fig. 1(b)), whereas the exact material properties and geometry of the inclusions was numerically modelled using COMSOL (as per Fig. 1(a)). The first peak at around 75 Hz for the voided coated shell is associated with a spring-mass resonance, whereby the shell acts as the mass and the compliant coating acts as the spring. Beyond the spring-mass resonance for the voided coated shell, global attenuation in the radiated acoustic pressure can be observed, attributed to the dramatic reduction in radiated sound at monopole resonance of the voids. Global attenuation for the coated shell with steel

inclusions is also observed, with the greatest attenuation occurring around dipole resonance of the scatterers. The greater reduction in sound pressure using a voided coating compared to a coating with hard inclusions is attributed to the fact that cavities in a soft medium effectively decouple the shell from the water, while the coating with hard inclusions is strongly coupled with the surrounding water. Contour plots at the spring-mass resonance, monopole resonance of the voids and dipole resonance of the steel scatterers are shown in Fig 2(a). The acoustic pressure distribution at the spring-mass resonance reveals that the coated shell is in translational motion in the same direction as the applied force, resulting in an acoustic dipole radiation pattern in the exterior domain. In Fig. 2(a), the shell has a vacuous interior. Figure 2(b) shows that when the interior cavity of the shell is air of density ρ_{int} = 1.225 kg/m^3 and sound speed c_{int}= 343(1-0.001i) m/s, internal acoustic resonances occur. The internal acoustic resonances are denoted by (p,q) modes, where p is the number of plane diametral nodal lines and q is the number of cylindrical nodal lines concentric with the cylinder axis. Figure 2(b) displays the pressure distributions within the shell cavity at the (1,0), (0,1) and (1,1) internal acoustic resonances. As frequency increases, the peaks associated with the internal acoustic resonances decrease in amplitude and eventually disappear, attributed to increasing radiation damping of the acoustic radiation modes of the shell in water. Comparison of Figs. 2(a) and 2(b) reveals that the internal acoustic resonances have negligible effect on the vibroacoustic response of the coated shell. In subsequent results, air in the interior cavity is neglected.

To analyse the acoustic responses for the coated shell in greater detail, the individual contributions to the radiated pressure for the lowest spectral orders are plotted in Fig. 3. For the voided coated shell in Fig. 3(a), the $n = 0$ spectral order which corresponds to axisymmetric (breathing) motion of the shell has negligible contribution to the spring-mass resonance. Contributions by successive spectral orders $n \geq 1$ to the spring-mass resonance can be observed, with the greatest contribution by the $n = 1$ spectral order associated with bending motion of the shell. Beyond the spring-mass resonance, distinct peaks in the structure-borne sound are associated with the circumferential modes of a coated shell in air. This is attributed to the fact that the voided coated shell becomes decoupled from the surrounding water. The decoupling mechanisms associated with the layer of voids are investigated in detail in the subsequent section. Beyond the peak for each spectral order, all contributions from the individual circumferential modes converge and as such, have similar contributions to the radiated sound. Figure 3(a) also shows that a trough in the radiated pressure at the monopole resonance of around 486 Hz occurs at all spectral orders. Figure 3(b) shows that the radiated pressure for a coated cylindrical shell with hard inclusions follows a similar trend to the response for an uncoated shell submerged in a heavy fluid. The contributions by the shell circumferential resonances to the radiated sound are less obvious due to strong coupling between the coated shell and the surrounding water. A sharp reduction in the

radiated pressure for a coated shell with voids or hard inclusions occurs at the ring frequency of the shell and its integer multiples. This is attributed to trapping of acoustic energy along the shell circumference which is subsequently dissipated due to structural damping of the shell [76]. The ring frequency of a cylindrical shell can be predicted using $f_R = c_L/2\pi a$, where $c_L = \sqrt{E_s/\rho_s(1-v_s^2)}$ is the longitudinal wave speed of the shell. Table 1 lists the predicted ring frequency and integer multiples, as well as the frequencies obtained at the troughs for the uncoated shell submerged in water, the coated shell with voids and the coated shell with hard inclusions. Comparison of the predicted and observed ring frequencies for the uncoated and coated shells reveals that the effect of heavy fluid loading or the presence of a coating with different inclusion material does not have a significant influence on the ring frequency of a shell, as previously observed [12,17,76,77]. Above the ring frequency, the radiated pressure from all spectral orders for the coated cylindrical shell with hard inclusions converge. A similar finding has also been reported by Maxit et al. [78] for an uncoated shell submerged in a heavy fluid.

Table 1 Predicted and observed ring frequencies for the uncoated and coated shells.

Predicted ring frequency (Hz)	Uncoated cylindrical shell in water (Hz)	Coated cylindrical shell with voids (Hz)	Coated cylindrical shell with hard inclusions (Hz)
865.7	865.6	865.3	865.6
1731.4	1730.4	1729.1	1730.2
2597.1	2594.0	2589.5	2596.2

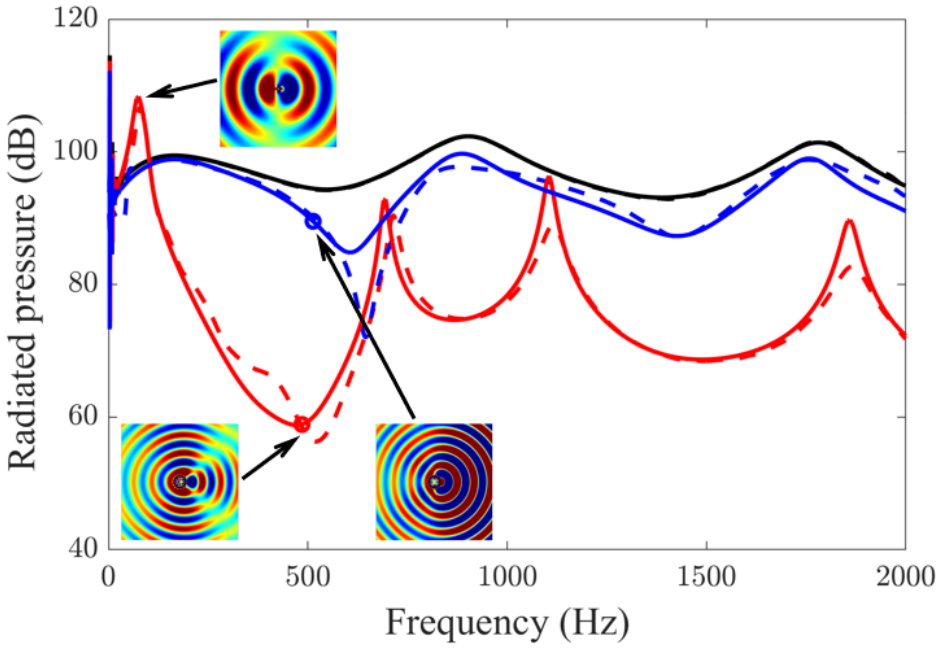

(a)

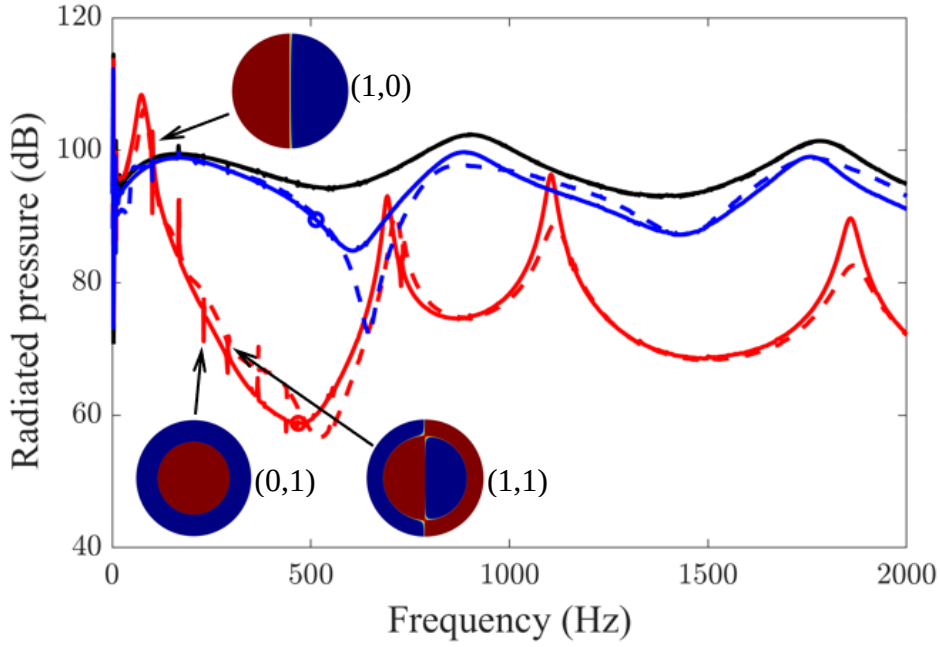

(b)

Figure 2 Radiated acoustic pressure (dB ref 1μPa) from an uncoated shell (black line), a shell with a coating embedded with 50 voids of 5 cm diameter (red line) or 110 hard inclusions of 5 cm diameter (blue line), obtained analytically (solid lines) and numerically (dashed lines). The shell has (a) a vacuous cavity or (b) an air filled cavity. The monopole and dipole resonances are respectively indicated by red and blue circles. Contour plots of the exterior pressure at the spring-mass resonance, monopole resonance of the voids and dipole resonance of the hard inclusions are shown in (a). Contour plots of the pressure distribution within the shell cavity at the (1,0), (0,1) and (1,1) acoustic resonances are shown in (b). Maximum and minimum acoustic pressures are represented by red and blue, respectively.

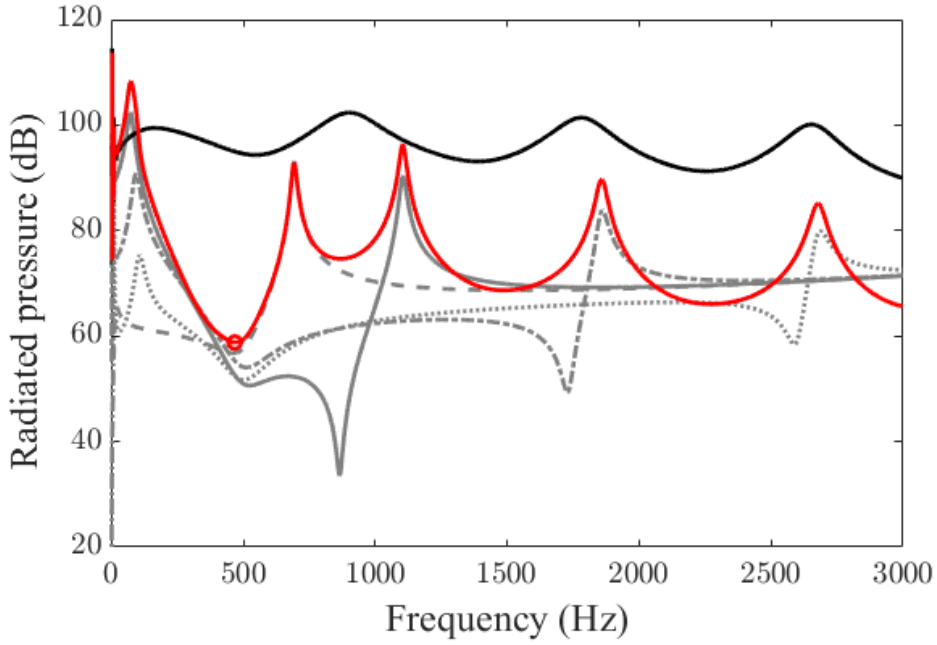

(a)

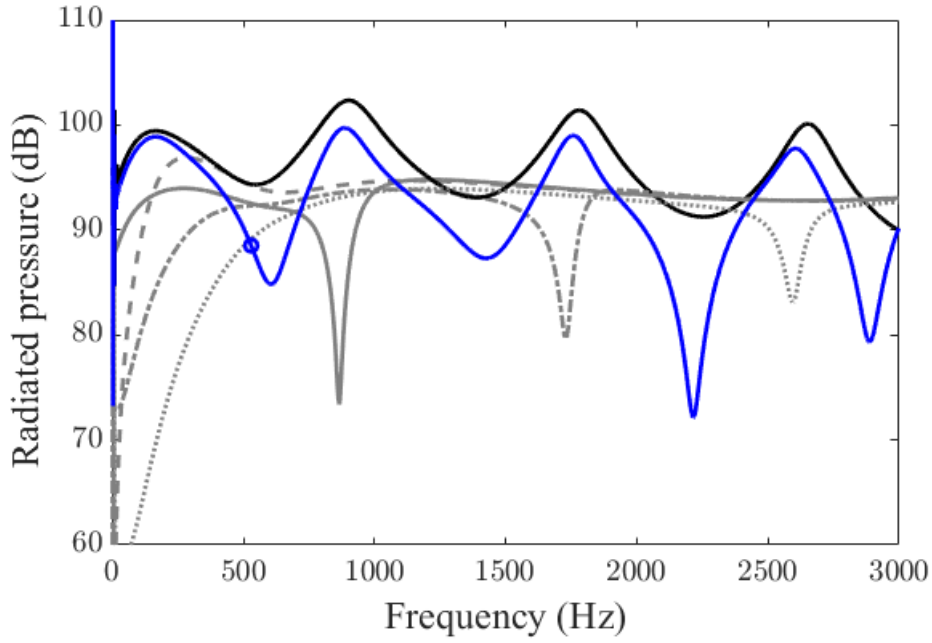

(b)

Figure 3 Radiated acoustic pressure (dB ref 1μPa) from an uncoated shell (black line), a shell with a coating embedded with (a) 50 voids of 5 cm diameter (red line) and (b) 110 hard inclusions of 5 cm diameter (blue line), as well as the individual contributions from the lowest spectral orders corresponding to $n = 0$ (grey dashed lines), $n = 1$ (grey solid lines), $n = 2$ (grey dashed-dot lines) and $n = 3$ (grey dotted lines). The monopole and dipole resonances are respectively indicated by red and blue circles.

3.2 Multiple layers of resonant inclusions

The combined effects of voids and hard inclusions in a multilayered coating comprising alternating homogeneous and homogenised layers are now investigated. Figure 4 presents schematic diagrams of four coating designs considered in this study. Designs A and B correspond to coatings composed of two layers of inclusions of the same material. Designs C and D correspond to coatings composed of two layers of inclusions of different materials. The coatings have a thickness of h_c = 0.2 m, which is double the thickness of the coating with a single layer of resonant inclusions. The distance from the shell surface to the interior layer of inclusions is the same as for the coating with a single layer of inclusions. The circumferential location between two homogenised layers corresponds to half the total thickness of the coating.

Figure 5 presents the radiated acoustic pressure for the different coating designs obtained analytically using the homogenisation approach presented here, and numerically using the finite element method. The same geometric properties of the inclusions in each layer as for a coating with a single layer of inclusions were used, corresponding to 50 voids and 110 hard inclusions of 5 cm diameter. The effective thickness of the homogenised layers for the four coating designs are listed in Table 2. The effective thickness of the outer layers is reduced compared to that of the inner layers of the same inclusion material, due to the increase in lattice spacing of the equispaced inclusions. Close agreement between results obtained analytically and numerically can be observed for all four coating designs. For coatings comprising one or two layers of voids (designs A, C, D), the presence of the low frequency spring-mass resonance is observed. For two layers of voids (design A), the spring-mass resonance is lower than for one layer of voids in proximity to the shell surface (design C), due to a reduction in stiffness of the coating. A layer of hard inclusions in proximity to the shell surface (design D) results in an increase in overall mass of the system and a corresponding reduction in the spring-mass resonance. Similar to a coating with a single layer of hard inclusions, the spring-mass resonance does not exist for a coating with two layers of hard inclusions (design B).

For coating designs A and C, sharp peaks in the radiated sound occurring at similar frequencies can be observed. We herein show that beyond the layer of voids in proximity to the shell surface, the coated shell is decoupled from the surrounding water. To investigate this decoupling effect, Fig. 6(a) compares the total acoustic response for the coated shells of designs A and C submerged in water, with the individual contributions to the radiated pressure from the lowest order circumferential modes of a uniformly coated shell in air. The thickness of the uniform coating for the shell in air is equal to the distance from the shell surface to the inner layer of voids for the coated shell in water. Results show that the peaks for each circumferential mode of a uniformly coated shell in air are in alignment with the corresponding circumferential resonances of the coated shells in water. The decoupling mechanism by the voids can be further verified by

examining the acoustic response for coating design D, corresponding to a layer of hard inclusions in proximity to the shell surface and an outer layer of voids. Figure 6(b) compares the acoustic performance for a coated shell of design D submerged in water with the individual contributions to the radiated sound from the circumferential resonances of a shell in air and coated with a single homogenised layer of hard inclusions. In this case, the total thickness of the coating for the shell in air is equal to the distance from the shell surface to the outer layer of voids for the coated shell in water. Figure 6(b) shows that the circumferential resonances for the coated shells in air and in water align, which indicates that beyond the outer layer of voids, the coated shell of design D is decoupled from the surrounding water.

Table 2 Effective thickness of homogenised layers for different coating designs.

	Effective thickness (mm)	
	Inner layer	Outer layer
Coating design A	15.9	14.3
Coating design B	51.7	42.0
Coating design C	15.9	42.0
Coating design D	51.7	14.3

Figure 7 presents the acoustic pressure for the four coating designs obtained analytically as a function of both frequency and distance from the shell surface. Regions of maximum and minimum radiated sound occur at the frequencies of the peaks and troughs in Fig. 5. For coatings comprising one or two layers of voids corresponding to designs A, C, D in Figs, 7(a), 7(c), 7(d), respectively, high sound pressure levels at low frequencies can be observed due to the introduction of a spring-mass resonance. These figures also show strong blocking of sound transmission at each layer of voids. For a layer of voids in proximity to the shell surface (designs A and C) and for an outer layer of voids (design D), the coated shell becomes decoupled from the surrounding water, as discussed previously. As a result, distinct peaks of maximum pressure analogous to circumferential resonances of a coated shell in air can be observed. For coating design B composed of two layers of hard inclusions (Fig. 7(b)), the coated shell is strongly coupled with water. The lowest radiated sound occurs around the dipole resonance frequency.

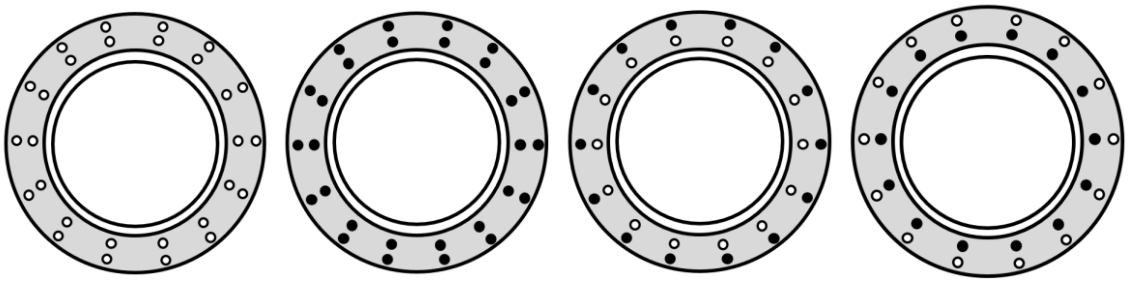

(a) (b) (c) (d)

Figure 4 Schematic diagrams for different coating designs (not to scale), corresponding to (a) design A (two layers of voids), (b) design B (two layers of hard inclusions), (c) design C (a layer of voids in proximity to the shell and an outer layer of hard inclusions) and (d) design D (a layer of hard inclusions in proximity to the shell and an outer layer of voids).

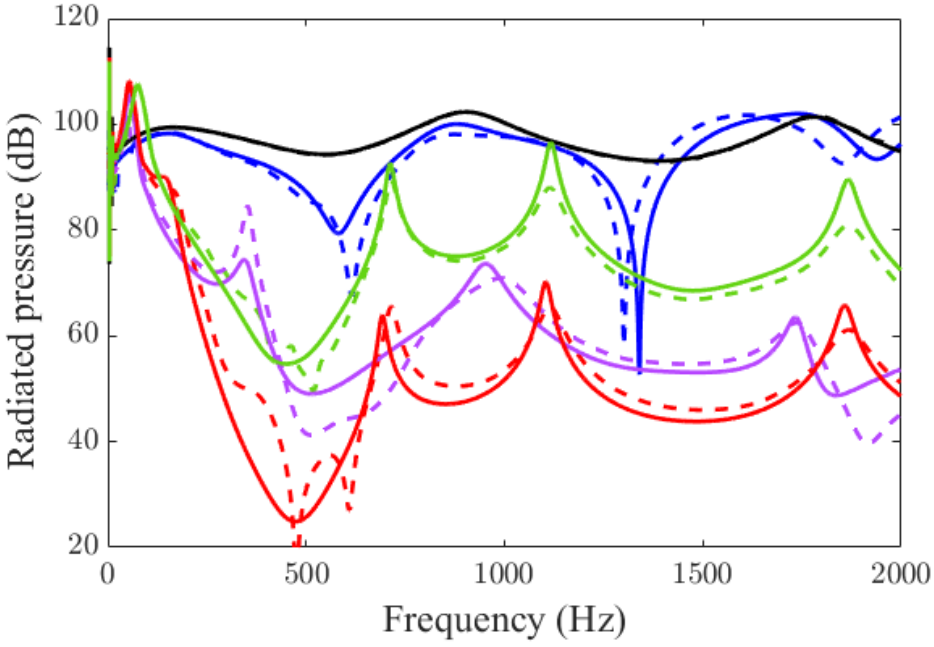

Figure 5 Radiated acoustic pressure (dB ref 1μPa) from an uncoated shell (black line), a coated shell of design A (red line), design B (blue line), design C (green line) and design D (purple line). Results are obtained analytically (solid lines) and numerically (dashed lines).

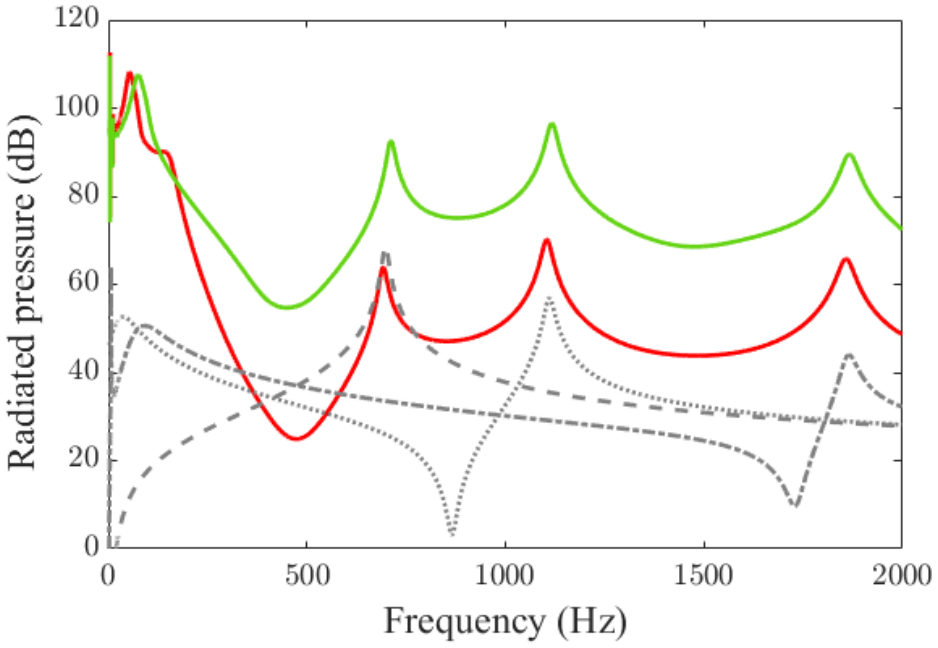

(a)

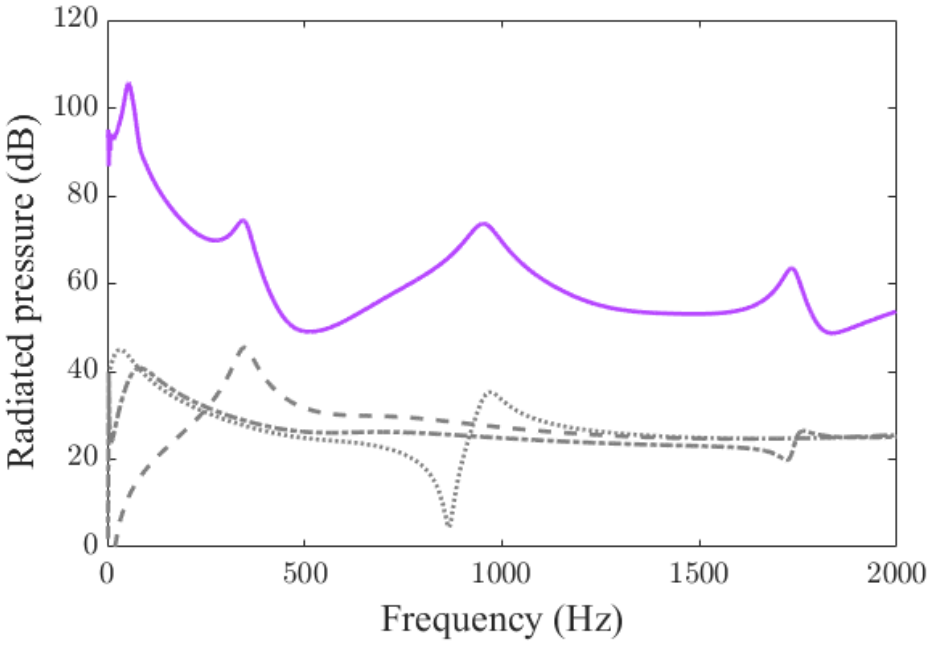

(b)

Figure 6 (a) Radiated acoustic pressure (dB ref 1μPa) from a coated shell of design A (red line) and design C (green line). Radiated acoustic pressure (dB ref 20 μPa) from the individual circumferential modes $n = 0$ (grey dashed line), $n = 1$ (grey dotted line), $n = 2$ (grey dashed-dot line) of a uniformly coated shell in air. (b) Radiated acoustic pressure (dB ref 1μPa) from a coated shell of design D (purple line). Radiated acoustic pressure (dB ref 20μPa) from the individual circumferential modes $n = 0$ (grey dashed line), $n = 1$ (grey dotted line), $n = 2$ (grey dashed-dot line) of a coated shell with hard inclusions in air.

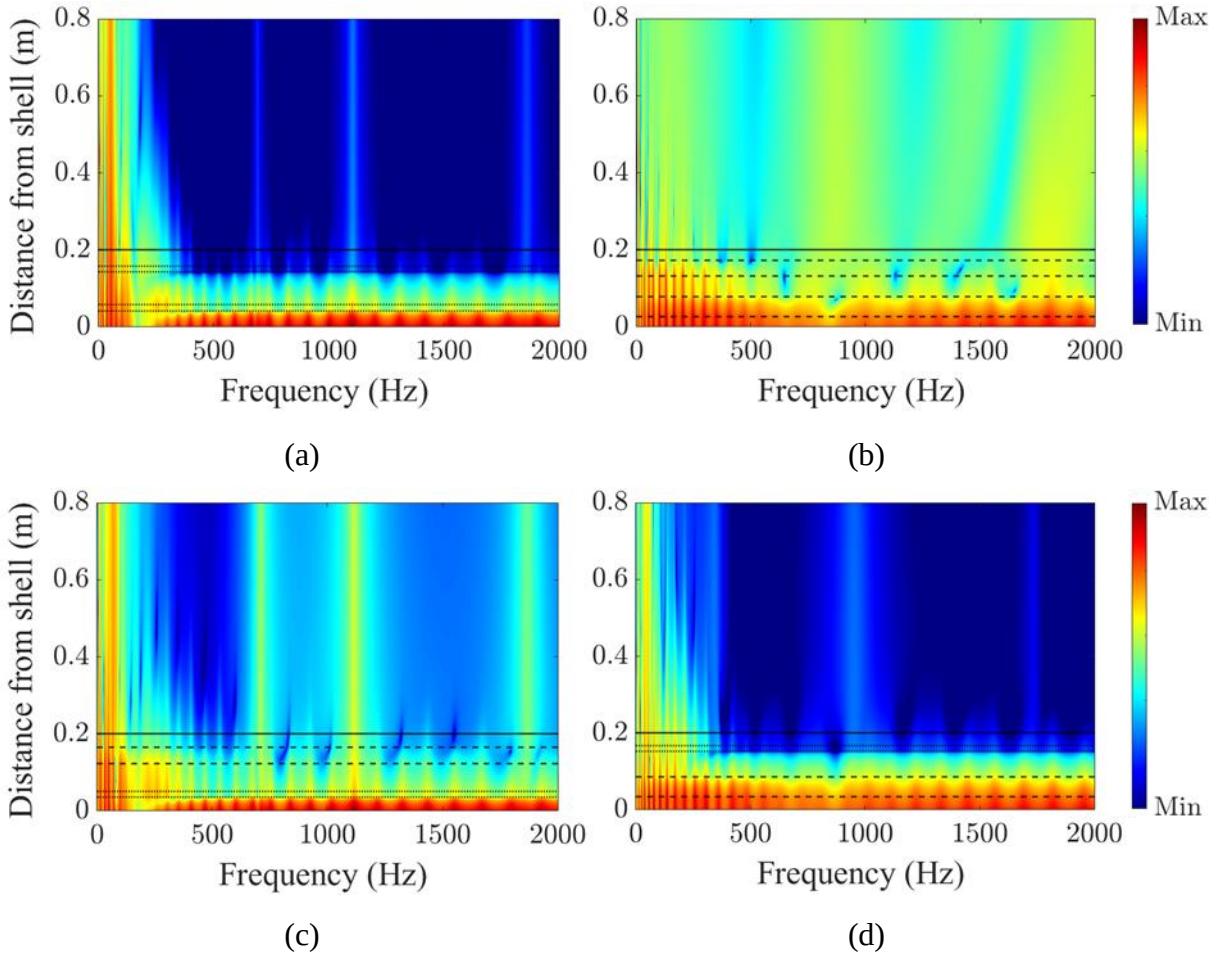

Figure 7 Acoustic pressure (dB ref 1μPa) as a function of distance from the shell surface measured at $\theta = \pi$ for a coated shell of (a) design A, (b) design B, (c) design C and (d) design D. The homogenised layers of voids and hard inclusions are indicated by black dotted and dashed lines respectively. The exterior surface of the coating is indicated by a black solid line.

3.3 Tuning of local resonances for single and multiple layers of resonant inclusions

The effect of tuning the resonance frequencies of the voids and hard inclusions on the acoustic performance of the coating is now investigated by varying the size and number of the inclusions. The monopole and dipole resonances for a single layer of voids and hard inclusions in a coating are tuned to target a similar frequency. The local resonances are then tuned to target different frequencies. The physical insights observed from tuning the resonance frequency in a coating comprising a single layer of inclusions are then utilised to understand the effects of tuning the resonance frequencies in the multilayered coating designs.

In Fig. 8(a), the local resonances of a single layer of voids (left column) and hard inclusions (right column) are tuned to a similar frequency of around 500 Hz using different combinations of the size and number of inclusions, ranging from a larger number of small sized scatterers to a smaller number of larger sized scatterers. Using a reduced number of larger sized inclusions results in greater reduction in the radiated pressure at the corresponding monopole and dipole resonances. Greater global reduction in the radiated sound beyond the monopole and dipole resonances occurs.

This is attributed to the fact that larger sized inclusions result in greater wave scattering, which in turn leads to strong blocking of sound waves by the coating composed of voids and greater conversion of sound waves to shear waves by the coating composed of hard inclusions. Figure 8(a)(left) also shows that increasing the void diameter results in a decrease in the frequency of the spring-mass resonance. This is attributed to the fact that the effective stiffness of the coating decreases with an increase in void diameter while the effective mass contributed by the cylindrical shell remains unchanged.

Figure 8(b) presents the radiated sound pressure for a single layer of voids and hard scatterers with a fixed diameter of 5 cm. The number of inclusions is varied to tune the monopole resonance of the voids (left column) and dipole resonance of the hard inclusions (right column) to different frequencies. Increasing the number of inclusions reduces the lattice spacing, resulting in resonances occurring at higher frequencies. Increasing the local resonance frequency of the inclusions results in greater reduction in the radiated pressure around and beyond the resonance frequency. This is attributed to increased resonance coupling as well as enhanced wave scattering by inclusions in proximity [37,42]. Similar results can also be obtained for a fixed number of inclusions and increasing the diameter of the voids or hard scatterers (results not shown here). It is further shown in Fig. 8(b)(left) that a decrease in the frequency of the spring-mass resonance occurs when the number of voids is increased, attributed to a decrease in the effective stiffness of the coating. Comparison of the spring-mass resonances in Figs. 8(a)(left) and 8(b)(left) reveals that the frequency of the spring-mass resonance is significantly affected by the size of the voids, and to a lesser degree, by the number of voids.

For the multilayered coating designs, the resonance frequency of the outer layer of inclusions is kept constant, while the resonance frequency of the inner layer is tuned by varying the size and number of the inclusions. Figure 8(c)(left) presents the radiated sound for coating designs A and C composed of an inner layer of voids, while Fig. 8(c)(right) presents the radiated sound for coating designs B and D composed of an inner layer of hard inclusions. Figure 8(c)(left) shows that when the inner layer is tuned to a similar monopole resonance of around 500 Hz using a smaller number of larger sized voids (dashed lines), greater reduction in radiated sound occurs around and beyond the resonance frequency, corroborating the results observed in Fig. 8(a)(left). Figure 8(c)(left) also reveals that when the inner layer of voids is tuned to a higher resonance frequency (dotted lines), greater reduction in radiated sound occurs beyond the resonance frequency, corroborating the trends observed in Fig. 8(b)(left). In Fig. 8(c)(right), the inner layer of hard inclusions is tuned to a similar dipole resonance of around 500 Hz using a smaller number of larger sized scatterers (dashed lines), or to a higher dipole resonance using a greater number of scatterers (dotted lines). Tuning the dipole resonance of the hard inclusions to a similar or higher frequency yields global reduction in the radiated sound for coating design B. In contrast, tuning

the dipole resonance of the hard inclusions to a similar or higher frequency in coating design D only yields an incremental reduction in radiated sound, attributed to decoupling of the coated shell from the surrounding water due to the outer layer of voids.

4. Conclusions

The radiated sound from a submerged cylindrical shell with a multilayered coating embedded with resonant inclusions has been presented. Coating designs composed of a soft compliant material with one or two layers of voids and/or hard inclusions were considered. The layers were homogenised using effective medium approximation theory, and the coatings were modelled as an equivalent fluid comprising alternating homogeneous and homogenised layers. The distribution of the homogenised layers was observed to significantly affect the radiated sound. For coating designs composed of voids only or both voids and hard inclusions, a low frequency spring-mass resonance was introduced. Beyond the spring-mass resonance, global attenuation in the radiated sound was achieved, attributed to effective decoupling of the shell from the water and significant reduction in the radiated sound around monopole resonance of the voids. A coating embedded with hard inclusions only was observed to be strongly coupled with the surrounding water, with the greatest reduction in radiated sound occurring around dipole resonance of the scatterers.

The influence of tuning the resonance frequencies of the voids and hard inclusions was investigated by varying the size and number of inclusions. Increasing the size of the inclusions or shifting the local resonance to a higher frequency yielded greater reduction in the radiated pressure around and beyond the resonance frequency. The acoustic performance of a coating composed of both voids and hard inclusions is more sensitive to variation in the monopole resonance of the voids compared to variation in the dipole resonance of the hard inclusions.

In this work, we have shown that a multilayered coating embedded with resonant inclusions can reduce sound radiation from a submerged cylindrical shell over a broad frequency range. Our future work will extend the current two-dimensional model to consider the vibroacoustic response of a coated cylindrical shell of finite length. A further focus of our future work is to investigate the radiated sound from a coated cylindrical shell excited by a turbulent boundary layer and examine the effectiveness of a resonant coating to absorb flow-induced noise.

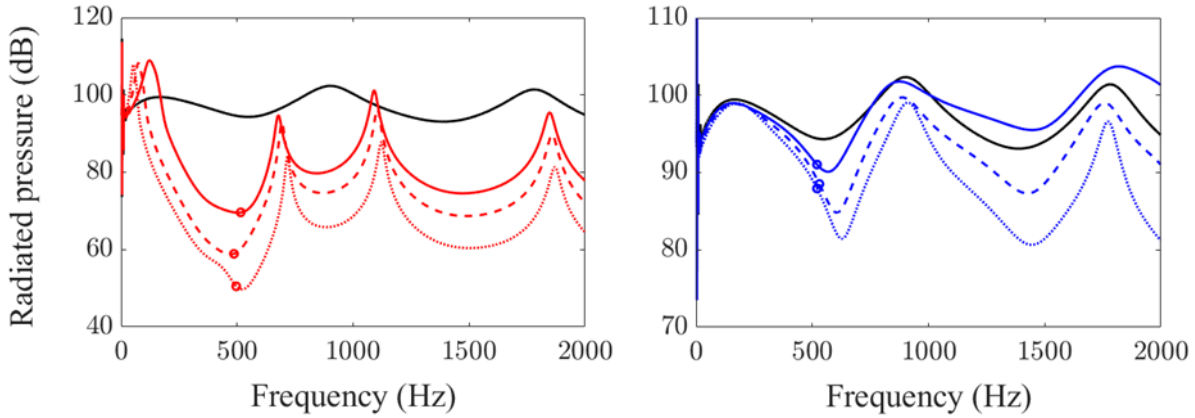

(a)

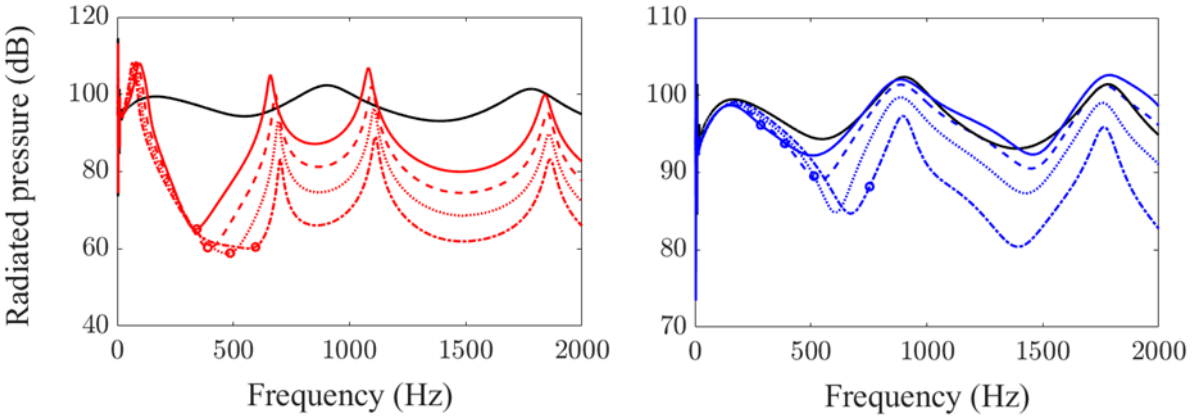

(b)

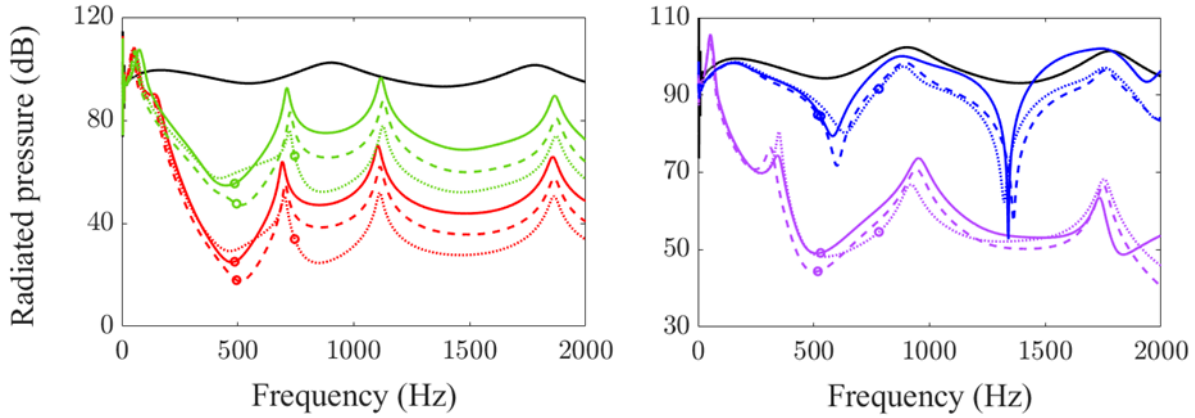

(c)

Figure 8 Radiated acoustic pressure (dB ref 1μPa) from an uncoated shell (black line), a shell with a coating embedded with (a)(left) 52 voids of 3 cm diameter (solid red line), 50 voids of 5 cm diameter (dashed red line) and 48 voids of 7 cm diameter (dotted red line); (a)(right) 154 hard inclusions of 3 cm diameter (solid blue line), 110 hard inclusions of 5 cm diameter (dashed blue line) and 84 hard inclusions of 7 cm diameter (dotted blue line); (b)(left) 30 (solid red line), 40 (dashed red line), 50 (dotted red line) and 60 (dotted-dashed red line) voids of 5 cm diameter; (b)(right) 90 (solid blue line), 100 (dashed blue line), 110 (dotted blue line) and 120 (dotted-dashed blue line) hard inclusions of 5 cm diameter; (c)(left) a coated shell of designs A and C (solid lines), frequency tuning using 48 voids of 7 cm diameter (dashed lines) and 70 voids of 5 cm diameter (dotted lines); (c)(right) a coated shell of designs B and D (solid lines), frequency tuning using 84 hard inclusions of 7 cm diameter (dashed lines) and 120 hard inclusions of 5 cm diameter (dotted lines). The tuned resonances of the inclusions are indicated by circles.

Appendix A Effective properties of a homogenised layer of resonant inclusions

A 1.1 Effective properties of a homogenised layer of voids

The effective geometric and material properties of a homogenised layer arising from a planar array of voids in a square lattice embedded in a soft material have been derived in our previous work and are given here for completeness of the current study. We herein employ the same effective geometric and material properties for the homogenised circumferential layer of voids. We show that this approach is valid when the radius of the cylindrical shell is much greater than the diameter of the inclusions and spacing between adjacent inclusions. The homogenisation models adopted in this work are suitable in the long wavelength limit, where the acoustic wavelength should be much larger than the size and spacing between the adjacent resonant inclusions [36,39]. The effective thickness is given by [36]

$$h_{\mathrm{eff},v} = \frac{2d_v}{\pi} \ln \sec\left(\frac{\pi a_v}{d_v}\right), \tag{A1}$$

where a_v is the radius of the voids and d_v is the circumferential distance between adjacent voids. The effective density is given by [36]

$$\rho_{\mathrm{eff},v} = \rho_c \left(1 - \frac{f_v d_v}{h_{\mathrm{eff},v}}\right), \tag{A2}$$

where $f_v = \pi(a_v/d_v)^2$ is the filling fraction associated with a planar array of voids in a square lattice. The effective longitudinal modulus for the homogenised layer of voids is dependent on the monopole resonance frequency of a single void in an infinite elastic medium ω_v and monopole resonance frequency of voids in an array Ω_v, given by [36]

$$\kappa_{\mathrm{eff},v} = \frac{\kappa_c(1-f_v)}{\left(\frac{f_v d_v}{h_{\mathrm{eff},v}}\right)\left(\left(\frac{\lambda_c}{\mu_c}+2\right)/\left(1-\left(\frac{\omega}{\Omega_v}\right)^2\right)+1\right)+(1-f_v)}, \tag{A3}$$

where λ_c and μ_c are the first and second Lamé constants. The expressions for ω_v and Ω_v are given by [37]

$$\omega_v = \frac{2c_s}{a_v\sqrt{0.23 + 2\ln\left(\frac{c_l}{c_s}\right)}}, \tag{A4}$$

$$\Omega_v = \frac{\omega_v}{\sqrt{1-\left(\frac{2a_v}{d_v}\right)^{-0.06\ln\left(\frac{2a_v}{d_v}\right)}}}. \tag{A5}$$

where $c_l = \sqrt{\kappa_c/\rho_c}$, $c_s = \sqrt{\mu_c/\rho_c}$ are the longitudinal and shear wave speeds in the coating and $c_l \gg c_s$ for a soft elastic material.

A 1.2 Effective properties of a homogenised layer of hard inclusions

Similar to the previous section, the effective properties of a homogenised layer composed of a planar array of hard scatterers in a square lattice embedded in a soft material are utilised as the effective geometric and material properties for the homogenised circumferential layer of hard scatterers. The effective properties have been derived previously and are also given here for completeness of the current study. The hard inclusions have radius a_h, density ρ_h and longitudinal modulus κ_h, and are equispaced along the circumference by distance d_h. The effective thickness $h_{\text{eff},h}$ associated with the layer of hard inclusions is obtained using the same expression given by Eq. (A1), with a_v replaced by a_h and d_v replaced by d_h.

The effective density of the homogenised layer comprising hard scatterers is a frequency dependent complex term denoted by $\rho_{\text{eff},h} = \rho'_{\text{eff},h} - \mathrm{i}\rho''_{\text{eff},h}$. The real and imaginary components are given by [79]

$$\rho'_{\text{eff},h} = \frac{\rho_c d_h}{h_{\text{eff},h}}\left(1 + f_h(\delta_h - 1)\frac{\left(\left(\frac{\Omega_h}{\omega}\right)^2 - \frac{1+m_h}{\delta_h+m_h}\right)\left(\left(\frac{\Omega_h}{\omega}\right)^2 - 1\right) + \left(\frac{\psi_h}{\omega}\right)^2}{\left(\left(\frac{\Omega_h}{\omega}\right)^2 - 1\right)^2 + \left(\frac{\psi_h}{\omega}\right)^2} + \frac{h_{\text{eff},h} - d_h}{d_h}\right), \tag{A6}$$

$$\rho''_{\text{eff},h} = \frac{\rho_c d_h}{h_{\text{eff},h}}\left(\frac{f_h \psi_h (\delta_h - 1)^2}{\omega(\delta_h + \beta_h)\left(\left(\left(\frac{\Omega_h}{\omega}\right)^2 - 1\right)^2 + \left(\frac{\psi_h}{\omega}\right)^2\right)}\right), \tag{A7}$$

where $f_h = \pi(a_h/d_h)^2$ is the filling fraction, $\delta_h = \rho_h/\rho_c$ is the ratio of the density of the hard inclusions to that of the host elastic medium, $m_h = \frac{1+f_h}{1-f_h}$, ψ_h is the effective damping for which an expression can be found in Ref. 39, and Ω_h corresponds to the dipole resonance frequency for hard inclusions in an array given by [79]

$$\Omega_h = \sqrt{\frac{K_{\text{eff},h}}{\rho_c \pi a_h^2 (\delta_h + m_h)}}, \tag{A8}$$

where K_{eff} is the effective stiffness coefficient given by [39]

$$K_{\text{eff},h} = \frac{8\pi\mu_c'(1+f_h^2)}{(1+f_h^2)\ln(1/f_h)+(f_h^2-1)}, \tag{A9}$$

where μ_c' is the real part of the shear modulus of the elastic coating. The effective longitudinal modulus of the homogenised layer composed of hard scatterers is given by [39]

$$\kappa_{\text{eff},h} = \frac{\kappa_c\kappa_h h_{\text{eff},h}}{f_h d_h(\kappa_c-\kappa_h)+h_{\text{eff},h}\kappa_h}. \tag{A10}$$

Appendix B Non-zero terms in matrix A

The non-zero terms in matrix **A** are given in what follows. The first number in the subscript of each element represents the matrix row and the second number in the subscript represents the matrix column. The non-zero terms in matrix **A** are normalised to prevent numerical underflow and overflow of Bessel and Hankel functions, respectively [80].

$$a_{11} = J_n(k_c a), \tag{B1}$$

$$a_{12} = H_n^1(k_c a), \tag{B2}$$

$$a_{17} = \frac{k_{\text{int}}}{\omega^2\rho_{\text{int}}}\left(\left(Dn^4+D\beta^2-\omega^2\rho_s h_s+D(1-2n^2)\right) - \frac{D\beta^2n^2G}{Gn^2-\omega^2\rho_s h_s}\right)J_n'(k_{\text{int}}a) - J_n(k_{\text{int}}a), \tag{B3}$$

$$a_{21} = \frac{k_c}{\omega^2\rho_c}\left(\left(Dn^4+D\beta^2-\omega^2\rho_s h_s+D(1-2n^2)\right) - \frac{D\beta^2n^2G}{Gn^2-\omega^2\rho_s h_s}\right)J_n'(k_c a) + J_n(k_c a), \tag{B4}$$

$$a_{22} = \frac{k_c}{\omega^2\rho_c}\left(\left(Dn^4+D\beta^2-\omega^2\rho_s h_s+D(1-2n^2)\right) - \frac{D\beta^2n^2G}{Gn^2-\omega^2\rho_s h_s}\right)H_n^{1'}(k_c a) + H_n^1(k_c a), \tag{B5}$$

$$a_{27} = -J_n(k_{\text{int}}a), \tag{B6}$$

$$a_{31} = -J_n(k_c R_1), \tag{B7}$$

$$a_{32} = -H_n^1(k_c R_1), \tag{B8}$$

$$a_{33} = J_n(k_{\text{eff}}R_1), \tag{B9}$$

$$a_{34} = H_n^1(k_{\text{eff}}R_1), \tag{B10}$$

$$a_{41} = -\frac{k_c J_n'(k_c R_1)}{\rho_c}, \tag{B11}$$

$$a_{42} = -\frac{k_c H_n^{1'}(k_c R_1)}{\rho_c}, \tag{B12}$$

$$a_{43} = \frac{k_{\text{eff}} J_n'(k_{\text{eff}} R_1)}{\rho_{\text{eff}}}, \tag{B13}$$

$$a_{44} = \frac{k_{\text{eff}} H_n^{1'}(k_{\text{eff}} R_1)}{\rho_{\text{eff}}}, \tag{B14}$$

$$a_{53} = -J_n(k_{\text{eff}} R_2), \tag{B15}$$

$$a_{54} = -H_n^1(k_{\text{eff}} R_2), \tag{B16}$$

$$a_{55} = J_n(k_c R_2), \tag{B17}$$

$$a_{56} = H_n^1(k_c R_2), \tag{B18}$$

$$a_{63} = -\frac{k_{\text{eff}} J_n'(k_{\text{eff}} R_2)}{\rho_{\text{eff}}}, \tag{B19}$$

$$a_{64} = -\frac{k_{\text{eff}} H_n^{1'}(k_{\text{eff}} R_2)}{\rho_{\text{eff}}}, \tag{B20}$$

$$a_{65} = \frac{k_c J_n'(k_c R_2)}{\rho_c}, \tag{B21}$$

$$a_{66} = \frac{k_c H_n^{1'}(k_c R_2)}{\rho_c}, \tag{B22}$$

$$a_{75} = -J_n(k_c R_3), \tag{B23}$$

$$a_{76} = -H_n^1(k_c R_3), \tag{B24}$$

$$a_{78} = H_n^1(k_{\text{ext}} R_3), \tag{B25}$$

$$a_{85} = -\frac{k_c J_n'(k_c R_3)}{\rho_c}, \tag{B26}$$

$$a_{86} = -\frac{k_c H_n^{1'}(k_c R_3)}{\rho_c}, \tag{B27}$$

$$a_{88} = \frac{k_{\text{ext}} H_n^{1'}(k_{\text{ext}} R_3)}{\rho_{\text{ext}}}. \tag{B28}$$

560

561

References

1. H. Shahsavari, M. Kornokar, R. Talebitooti, K. Daneshjou, The study of sound transmission through sandwich cylindrical shells with circumferentially corrugated cores filled with porous materials, Compos. Struct. 291 (2022) 115608. https://doi.org/10.1016/j.compstruct.2022.115608
2. J. Zhou, A. Bhaskar, X. Zhang, Sound transmission through double cylindrical shells lined with porous material under turbulent boundary layer excitation, J. Sound Vib. 357 (2015) 253-268. https://doi.org/10.1016/j.jsv.2015.07.014
3. H. Darvish Gohari, M. Zarastvand, R. Talebitooti, Acoustic performance prediction of a multilayered finite cylinder equipped with porous foam media, J. Vib. Control 26 (2022) 899-912. https://doi.org/10.1177/1077546319890025
4. R. Talebitooti, A. Choudari Khameneh, M. Zarastvand, M. Kornokar, Investigation of three-dimensional theory on sound transmission through compressed poroelastic sandwich cylindrical shell in various boundary configurations, J. Sandw. Struct. Mater. 21 (2018) 2313-2357. https://doi.org/10.1177/1099636217751562
5. Q. Zhang, Sound transmission through micro-perforated double-walled cylindrical shells lined with porous material, J. Sound Vib. 485 (2020) 115539. https://doi.org/10.1016/j.jsv.2020.115539
6. Y. Liu, C. He, On sound transmission through double-walled cylindrical shells lined with poroelastic material: Comparison with Zhou′s results and further effect of external mean flow, J. Sound Vib. 358 (2015) 192-198. https://doi.org/10.1016/j.jsv.2015.07.038
7. Y. Liu, C. He, Diffuse field sound transmission through sandwich composite cylindrical shells with poroelastic core and external mean flow, Compos. Struct. 135 (2016) 383-396. https://doi.org/10.1016/j.compstruct.2015.09.025
8. J. Zhou, A. Bhaskar, X. Zhang, The effect of external mean flow on sound transmission through double-walled cylindrical shells lined with poroelastic material, J. Sound Vib. 333 (2014) 1972-1990. https://doi.org/10.1016/j.jsv.2013.11.038
9. M. Zarastvand, M. Asadijafari, R. Talebitooti, Improvement of the low-frequency sound insulation of the poroelastic aerospace constructions considering Pasternak elastic foundation, Aerosp. Sci. Technol. 112 (2021) 106620. https://doi.org/10.1016/j.ast.2021.106620
10. M. Zarastvand, M. Ghassabi, R. Talebitooti, Prediction of acoustic wave transmission features of the multilayered plate constructions: A review, J. Sandw. Struct. Mater. 24 (2021) 218-293. https://doi.org/10.1177/1099636221993891

11. Y. Jin, X. Jia, Q. Wu, G. Yu, X. Zhang, S. Chen, L. Wu, Design of cylindrical honeycomb sandwich meta-structures for vibration suppression, Mech. Syst. Signal Process. 163 (2022) 108075. https://doi.org/10.1016/j.ymssp.2021.108075
12. Z. Liu, R. Rumpler, L. Feng, Investigation of the sound transmission through a locally resonant metamaterial cylindrical shell in the ring frequency region, J. Appl. Phys. 125 (2019) 115105. https://doi.org/10.1016/j.ymssp.2020.107179
13. Z. Liu, R. Rumpler, L. Feng, Locally resonant metamaterial curved double wall to improve sound insulation at the ring frequency and mass-spring-mass resonance, Mech. Syst. Signal Process. 149 (2021) 107179. https://doi.org/10.1016/j.ymssp.2020.107179
14. C. Ren, Q. Li, D. Yang, Quasi-static and sound insulation performance of a multifunctional cylindrical cellular shell with bidirectional negative-stiffness metamaterial cores, Int. J. Mech. Sci. 180 (2020) 105662. https://doi.org/10.1016/j.ijmecsci.2020.105662
15. M. Zarastvand, M. Asadijafari, R. Talebitooti, Acoustic wave transmission characteristics of stiffened composite shell systems with double curvature, Compos. Struct. 292 (2022) 115688. https://doi.org/10.1016/j.compstruct.2022.115688
16. K. Daneshjou, A. Nouri, R. Talebitooti, Sound transmission through laminated composite cylindrical shells using analytical model, Arch. Appl. Mech. 77 (2006) 363-379. https://doi.org/10.1007/s00419-006-0096-7
17. K. Daneshjou, A. Nouri, R. Talebitooti, Analytical model of sound transmission through orthotropic cylindrical shells with subsonic external flow, Aerosp. Sci. Technol. 13 (2009) 18-26. https://doi.org/10.1016/j.ast.2008.02.005
18. R. Talebitooti, M. Zarastvand, H. Gohari, Investigation of power transmission across laminated composite doubly curved shell in the presence of external flow considering shear deformation shallow shell theory, J. Vib. Control 24 (2017) 4492-4504. https://doi.org/10.1177/1077546317727655
19. G. Jin, C. Yang, Z. Liu, S. Gao, C. Zhang, A unified method for the vibration and damping analysis of constrained layer damping cylindrical shells with arbitrary boundary condition, Compos. Struct 130 (2015) 124-142. https://doi.org/10.1016/j.compstruct.2015.04.017
20. L. Zheng, Q. Qiu, H. Wan, D. Zhang, Damping analysis of multilayer passive constrained layer damping on cylindrical shell using transfer function method, J. Vib. Acoust. 136 (2014) 031001. https://doi.org/10.1115/1.4026614
21. H. Ma, W. Sun, D. Du, X. Liu, H. Liu, Nonlinear vibration analysis of double cylindrical shells coupled structure with bolted connection and partially attached constrained layer damping, Int. J. Mech. Sci. 223 (2022) 107270. https://doi.org/10.1016/j.ijmecsci.2022.107270

22. H. Gohari, M. Zarastvand, R. Talebitooti, A. Loghmani, M. Omidpanah, Radiated sound control from a smart cylinder subjected to piezoelectric uncertainties based on sliding mode technique using self-adjusting boundary layer, Aerosp. Sci. Technol. 106 (2020) 106141. https://doi.org/10.1016/j.ast.2020.106141
23. R. Talebitooti, H. Darvish Gohari, M. Zarastvand, A. Loghmani, A robust optimum controller for suppressing radiated sound from an intelligent cylinder based on sliding mode method considering piezoelectric uncertainties, J. Intell. Mater. Syst. Struct. 30 (2019) 3066-3079. https://doi.org/10.1177/1045389X19873412
24. A. Loghmani, M. Danesh, M. Kwak, M. Keshmiri, Vibration suppression of a piezo-equipped cylindrical shell in a broad-band frequency domain, J. Sound Vib. 411 (2017) 260-277. https://doi.org/10.1016/j.jsv.2017.08.051
25. C. Thongchom, P. Saffari, N. Refahati, P. Saffari, H. Pourbashash, S. Sirimontree, S. Keawsawasvong, An analytical study of sound transmission loss of functionally graded sandwich cylindrical nanoshell integrated with piezoelectric layers, Sci. Rep. 12 (2022) 1. https://doi.org/10.1038/s41598-022-06905-1
26. C. Li, Q. Han, Guided waves propagation in sandwich cylindrical structures with functionally graded graphene-epoxy core and piezoelectric surface layers, J. Sandw. Struct. Mater. 23 (2020) 3878-3901. https://doi.org/10.1177/1099636220959034
27. F. Mitri, Acoustic radiation force due to incident plane-progressive waves on coated cylindrical shells immersed in ideal compressible fluids, Wave Motion. 43 (2006) 445-457. https://doi.org/10.1016/j.wavemoti.2006.02.005
28. J. Sastry, M. Munjal, Response of a multi-layered infinite cylinder to a plane wave excitation by means of transfer matrices, J. Sound Vib. 209 (1998) 99-121. https://doi.org/10.1006/jsvi.1997.1262
29. G. Gaunaurd. Sonar cross section of a coated hollow cylinder in water, J. Acoust. Soc. Am. 61 (1977) 360-368. https://doi.org/10.1121/1.381313
30. S. Hasheminejad, N. Safari, Acoustic scattering from viscoelastically coated spheres and cylinders in viscous fluids, J. Sound Vib. 280 (2005) 101–125. https://doi.org/10.1016/j.jsv.2003.12.027
31. L. Flax, W. Neubauer, Acoustic reflection from layered elastic absorptive cylinders, J. Acoust. Soc. Am. 61 (1977) 307-312. https://doi.org/10.1121/1.381323
32. M. Zou, L. Jiang, S. Liu, Underwater acoustic radiation by structures arbitrarily covered with acoustic coatings, J. Sound Vib. 443 (2019) 748-763. https://doi.org/10.1016/j.jsv.2018.12.017

33. J. Cuschieri, D. Feit, Influence of circumferential partial coating on the acoustic radiation from a fluid-loaded shell, J. Acoust. Soc. Am. 107 (2000) 3196-3207. https://doi.org/10.1121/1.429347
34. B. Laulagnet, J. Guyader, Sound radiation from finite cylindrical shells, partially covered with longitudinal strips of compliant layer, J. Sound Vib. 186 (1995) 723-742. https://doi.org/10.1006/jsvi.1995.0485
35. J. Cuschieri, The modeling of the radiation and response Green's function of a fluid-loaded cylindrical shell with an external compliant layer, J. Acoust. Soc. Am. 119 (2006) 2150-2169. https://doi.org/10.1121/1.2173068
36. G. Sharma, A. Skvortsov, I. MacGillivray, N. Kessissoglou, Acoustic performance of gratings of cylindrical voids in a soft elastic medium with a steel backing, J. Acoust. Soc. Am. 141 (2017) 4694–4704. https://doi.org/10.1121/1.4986941
37. G. Sharma, A. Skvortsov, I. MacGillivray, N. Kessissoglou, Sound transmission through a periodically voided soft elastic medium submerged in water, Wave Motion, 70 (2017) 101-112. https://doi.org/10.1016/j.wavemoti.2016.10.006
38. S. Wang, B. Hu, Y. Du, Sound absorption of periodically cavities with gradient changes of radii and distances between cavities in a soft elastic medium, Appl. Acoust. 170 (2020) 107501. https://doi.org/10.1016/j.apacoust.2020.107501
39. G. Sharma, A. Skvortsov, I. MacGillivray, N. Kessissoglou, Acoustic performance of periodic steel cylinders embedded in a viscoelastic medium, J. Sound Vib. 443 (2019) 652-665. https://doi.org/10.1016/j.jsv.2018.12.013
40. J. Zhong, H. Zhao, H. Yang, Y. Wang, J. Yin, J. Wen, Theoretical requirements and inverse design for broadband perfect absorption of low-frequency waterborne sound by ultrathin metasurface, Sci. Rep. 9 (2019) 1181. https://doi.org/10.1038/s41598-018-37510-w
41. L. Huang, Y. Xiao, J. Wen, H. Zhang, X. Wen, Optimization of decoupling performance of underwater acoustic coating with cavities via equivalent fluid model, J. Sound Vib. 426 (2018) 244-257. https://doi.org/10.1016/j.jsv.2018.04.024
42. A. Skvortsov, G. Sharma, I. MacGillivray, N. Kessissoglou, Sound absorption by a metasurface comprising hard spheres in a soft medium, J. Acoust. Soc. Am. 150 (2021) 1448-1452. https://doi.org/10.1121/10.0005897
43. S. Ivansson, Anechoic coatings obtained from two- and three-dimensional monopole resonance diffraction gratings, J. Acoust. Soc. Am. 131 (2012) 2622-2637. https://doi.org/10.1121/1.3689852
44. M. Hinders, B. Rhodes, T. Fang, Particle-loaded composites for acoustic anechoic coatings, J. Sound Vib. 185 (1995) 219-246. https://doi.org/10.1006/jsvi.1995.0377

45. H. Zhao, Y. Liu, D. Yu, G. Wang, J. Wen, X. Wen, Absorptive properties of three-dimensional phononic crystal, J. Sound Vib. 303 (2007) 185-194. https://doi.org/10.1016/j.jsv.2007.01.004
46. H. Zhao, Y. Liu, J. Wen, D. Yu, X. Wen, Tri-component phononic crystals for underwater anechoic coatings, Phys. Lett. A 367 (2007) 224-232. https://doi.org/10.1016/j.physleta.2007.02.048
47. G. Gaunaurd, One-dimensional model for acoustic absorption in a viscoelastic medium containing short cylindrical cavities, J. Acoust. Soc. Am. 62 (1977) 298-307. https://doi.org/10.1121/1.381528
48. G. Gaunaurd, K. Scharnhorst, H. Überall, Giant monopole resonances in the scattering of waves from gas-filled spherical cavities and bubbles, J. Acoust. Soc. Am. 65 (1979) 573-594. https://doi.org/10.1121/1.382494
49. J. Wen, H. Zhao, L. Lv, B. Yuan, G. Wang, X. Wen, Effects of locally resonant modes on underwater sound absorption in viscoelastic materials, J. Acoust. Soc. Am. 130 (2011) 1201-1208. https://doi.org/10.1121/1.3621074
50. Y. Zhang, L. Cheng, Ultra-thin and broadband low-frequency underwater acoustic meta-absorber, Int. J. Mech. Sci. 210 (2021) 106732. https://doi.org/10.1016/j.ijmecsci.2021.106732
51. A.C. Hladky-Hennion, J.N. Decarpigny, Analysis of the scattering of a plane acoustic wave by a doubly periodic structure using the finite element method: Application to Alberich anechoic coatings, J. Acoust. Soc. Am. 90 (1991) 3356-3367. https://doi.org/10.1121/1.401395
52. P. Langlet, A.C. Hladky-Hennion, J.N. Decarpigny, Analysis of the propagation of plane acoustic waves in passive periodic materials using the finite element method, J. Acoust. Soc. Am. 98 (1995) 2792-2800. https://doi.org/10.1121/1.413244
53. H. Meng, J. Wen, H. Zhao, L. Lv, X. Wen, Analysis of absorption performances of anechoic layers with steel plate backing, J. Acoust. Soc. Am. 132 (2012) 69-75. https://doi.org/10.1121/1.4728198
54. J. Zhong, H. Zhao, H. Yang, J. Yin, J. Wen, On the accuracy and optimization application of an axisymmetric simplified model for underwater sound absorption of anechoic coatings, Appl. Acoust. 145 (2019) 104-111. https://doi.org/10.1016/j.apacoust.2018.10.005
55. H. Yang, Y. Xiao, H. Zhao, J. Zhong, J. Wen, On wave propagation and attenuation properties of underwater acoustic screens consisting of periodically perforated rubber layers with metal plates, J. Sound Vib. 444 (2019) 21-34. https://doi.org/10.1016/j.jsv.2018.12.031

56. H. Meng, J. Wen, H. Zhao, X. Wen, Optimization of locally resonant acoustic metamaterials on underwater sound absorption characteristics, J. Sound Vib. 331 (2012) 4406-4416. https://doi.org/10.1016/j.jsv.2012.05.027
57. K. Shi, G. Jin, T. Ye, Y. Zhang, M. Chen, Y. Xue, Underwater sound absorption characteristics of metamaterials with steel plate backing, Appl. Acoust. 153 (2019) 147-156. https://doi.org/10.1016/j.apacoust.2019.04.016
58. T. Wang, J. Liu, M. Chen, Underwater sound absorption of a meta-absorption layer with double negativity, Appl. Acoust. 181 (2021) 108182. https://doi.org/10.1016/j.apacoust.2021.108182
59. X. Jia, G. Jin, K. Shi, C. Bu, T. Ye, A hybrid acoustic structure for low-frequency and broadband underwater sound absorption, J. Low Freq. Noise Vib. Act. Control 0 (2022) 1-18. https://doi.org/10.1177/14613484221081846
60. L. Wang, C. Ma, J. Wu, A thin meta-structure with multi-order resonance for underwater broadband sound absorption in low frequency, Appl. Acoust. 179 (2021) 108025. https://doi.org/10.1016/j.apacoust.2021.108025
61. H. Yang, H. Zhao, J. Wen, Theory and numerical method for the effects of hydrostatic pressure on sound absorption of underwater acoustic coatings with air cavities, J. Sound Vib. 533 (2022) 116985. https://doi.org/10.1016/j.jsv.2022.116985
62. K. Shi, G. Jin, R. Liu, T. Ye, Y. Xue, Underwater sound absorption performance of acoustic metamaterials with multilayered locally resonant scatterers, Results Phys. 12 (2019) 132-142. https://doi.org/10.1016/j.rinp.2018.11.060
63. J. Zhong, H. Zhao, H. Yang, J. Yin, J. Wen, Effect of Poisson's loss factor of rubbery material on underwater sound absorption of anechoic coatings, J. Sound Vib. 424 (2018) 293-301. https://doi.org/10.1016/j.jsv.2018.02.022
64. Y. Gu, H. Zhong, B. Bao, Q. Wang, J. Wu, Experimental investigation of underwater locally multi-resonant metamaterials under high hydrostatic pressure for low frequency sound absorption, Appl. Acoust. 172 (2021) 107605. https://doi.org/10.1016/j.apacoust.2020.107605
65. D. Calvo, A. Thangawng, C. Layman, R. Casalini, S. Othman, Underwater sound transmission through arrays of disk cavities in a soft elastic medium, J. Acoust. Soc. Am. 138 (2015) 2537-2547. https://doi.org/10.1121/1.4931446
66. H. Zhao, J. Wen, D. Yu, X. Wen, Low-frequency acoustic absorption of localized resonances: Experiment and theory, J. Appl. Phys. 107 (2010) 023519. https://doi.org/10.1063/1.3284943
67. R. Lane, Absorption mechanisms for waterborne sound in Alberich anechoic layers, Ultrasonics, 19 (1981) 28-30. https://doi.org/10.1016/0041-624X(81)90029-9

68. V. Leroy, A. Bretagne, M. Fink, H. Willaime, P. Tabeling, A. Tourin, Design and characterization of bubble phononic crystals, Appl. Phys. Lett. 95 (2009) 171904. https://doi.org/10.1063/1.3254243
69. C. Cushing, P. Wilson, M. Haberman, C. Shen, J. Li, S. Cummer, Z. Tan, C. Ma, H. Du, N. Fang, Characterization of an underwater metamaterial made of aluminum honeycomb panels at low frequencies, J. Acoust. Soc. Am. 149 (2021) 1829-1837. https:// doi.org/10.1121/10.0003629
70. G. Jin, K. Shi, T. Ye, J. Zhou, Y. Yin, Sound absorption behaviors of metamaterials with periodic multi-resonator and voids in water, Appl. Acoust. 166 (2020) 107351. https://doi.org/10.1016/j.apacoust.2020.107351
71. G. Sharma, A. Skvortsov, I. MacGillivray, N. Kessissoglou, Sound absorption by rubber coatings with periodic voids and hard inclusions, Appl. Acoust. 143 (2019) 200-210. https://doi.org/10.1016/j.apacoust.2018.09.003
72. G. Sharma, A. Marsick, L. Maxit, A. Skvortsov, I. MacGillivray, N. Kessissoglou, Acoustic radiation from a cylindrical shell with a voided soft elastic coating, J. Acoust. Soc. Am. 150 (2021) 4308-4314. https://doi.org/10.1121/10.0008907
73. Y. Ke, L. Zhang, X. Zhao, M. Tao, An equivalent method for predicting acoustic scattering of coated shell using identified viscoelastic parameters of anechoic coating, Appl. Acoust. 179 (2021) 108071. https://doi.org/10.1016/j.apacoust.2021.108071
74. A.W. Leissa, Vibration of shells, American Institute of Physics, New York, 1993.
75. P.A. Martin, Multiple scattering: Interaction of time-harmonic waves with N obstacles, Cambridge University Press, 2006.
76. B. Laulagnet, J. Guyader, Modal analysis of a shell's acoustic radiation in light and heavy fluids, J. Sound Vib. 131 (1989) 397-415. https://doi.org/10.1016/0022-460X(89)91001-8
77. J. Scott, The free modes of propagation of an infinite fluid-loaded thin cylindrical shell, J. Sound Vib. 125 (1988) 241-280. https://doi.org/10.1016/0022-460X(88)90282-9
78. L. Maxit, M. Karimi, V. Meyer, N. Kessissoglou, Vibroacoustic responses of a heavy fluid loaded cylindrical shell excited by a turbulent boundary layer, J. Fluids Struct. 92 (2020) 102758. https://doi.org/10.1016/j.jfluidstructs.2019.102758
79. V. Fedotovskii, T. Vereschagina. Resonance dispersion of the longitudinal waves in disperse composites, Acoust. Phys. 56 (2010) 506–513. https://doi.org/10.1134/S1063771010040160
80. D. C. Ricks, H. Schmidt, A numerically stable global matrix method for cylindrically layered shells excited by ring forces, J. Acoust. Soc. Am. 95 (1994) 3339-3349. https://doi.org/10.1121/1.409953